Earth and Planetary Science Letters 576 (2021) 117169

Contents lists available at ScienceDirect

Earth and Planetary Science Letters

www.elsevier.com/locate/epsl

Timescales of magma transport in the Columbia River flood basalts, determined by paleomagnetic data

Joseph Biasi [a,b,c,*], Leif Karlstrom [c]

[a] California Institute of Technology, Pasadena, CA, USA
[b] Dartmouth College, Hanover, NH, USA
[c] University of Oregon, Eugene, OR, USA

ARTICLE INFO

Article history:
Received 17 January 2021
Received in revised form 7 August 2021
Accepted 16 August 2021
Available online xxxx
Editor: C.M. Petrone

Dataset link:
https://earthref.org/MagIC/19000

Dataset link: https://github.com/leifkarlstrom/dike_conductiveheating_1d

Keywords:
flood basalt
dike
paleomagnetism
mass extinction
magma transport
volcanology

ABSTRACT

Flood basalts represent major events in Earth History, in part because they are linked to large climate perturbations and mass extinctions. However, the durations of individual flood basalt eruptions, which directly impact potential environmental crises, are poorly constrained. Here we use a combination of paleomagnetic data and thermal modeling to create a magnetic geothermometer (MGT) that can constrain the active transport lifetime of magmatic conduits and intrusions. We apply the MGT technique to eight feeder dike segments of the Columbia River basalts (CRB), demonstrating that some dike segments were actively heating host rocks for less than one month, while other segments may have been active for several years. Results suggest that eruption rates, localized spatially along-strike of dike segments, were as high as 1–8 $km^3\,day^{-1}$. These results help contextualize field evidence for contrasting CRB eruption durations and suggest a pathway for constraining the tempo of global flood basalt magmatism that is beyond the resolution of geochronology.

1. Introduction

Throughout Earth History, emplacement of flood basalts often coincided with mass extinctions or major climate disturbances (Clapham and Renne, 2019). Individual flood basalt eruptions can release large amounts of carbon, sulfur, chlorine, fluorine, and mercury directly into the atmosphere (Thordarson and Self, 1996). If these volatiles are released over thousands of years, then their effects may be significantly muted through biogeochemical sequestration. However, if most of these volatiles are released in short-duration high-intensity pulses, they can have a major impact on the climate (Schmidt et al., 2016). Uncertainty in individual eruption durations is therefore a major barrier to understanding these events.

Current geochronological techniques can determine the amount of time that has passed between two discrete eruptions if they are not within error of each other (>10 kyr for the Columbia River Basalts or CRB; Kasbohm and Schoene, 2018) but cannot measure the duration of the eruptions themselves. Paleoclimate proxies in the sedimentary record commonly preserve the climatic or biological impact of these eruptions (e.g. Fendley et al., 2019), not the eruptions themselves, and sedimentation rates are too slow to capture such events in detail.

In this study, we use a combination of paleomagnetic data and thermal modeling to create a magnetic geothermometer (MGT) and show how it can be used to determine the duration of magma transport in dikes, sills, and other igneous intrusions. We apply the MGT technique to eight Columbia River flood basalt feeder dike segments to determine the duration of eruptions in this event.

2. Geologic background

From ~16.7 to ~6.2 Ma, ~210,000 km^3 of basalt and basaltic andesite (generally termed 'flood basalts') were erupted in the northwestern United States (Fig. 1a) (Reidel et al., 2013; Kasbohm and Schoene, 2018). The largest formation of the CRB, the Grande Ronde basalts (149,000 km^3), was erupted over a timespan of <400 kyr (Kasbohm and Schoene, 2018). This implies average eruption rates of ~0.37 km^3/year. In the CRB, mapping of flow fields suggest eruptions persist for more than a decade (e.g.

* Corresponding author at: Dartmouth College, Hanover, NH, USA.
E-mail address: biasi@dartmouth.edu (J. Biasi).

https://doi.org/10.1016/j.epsl.2021.117169

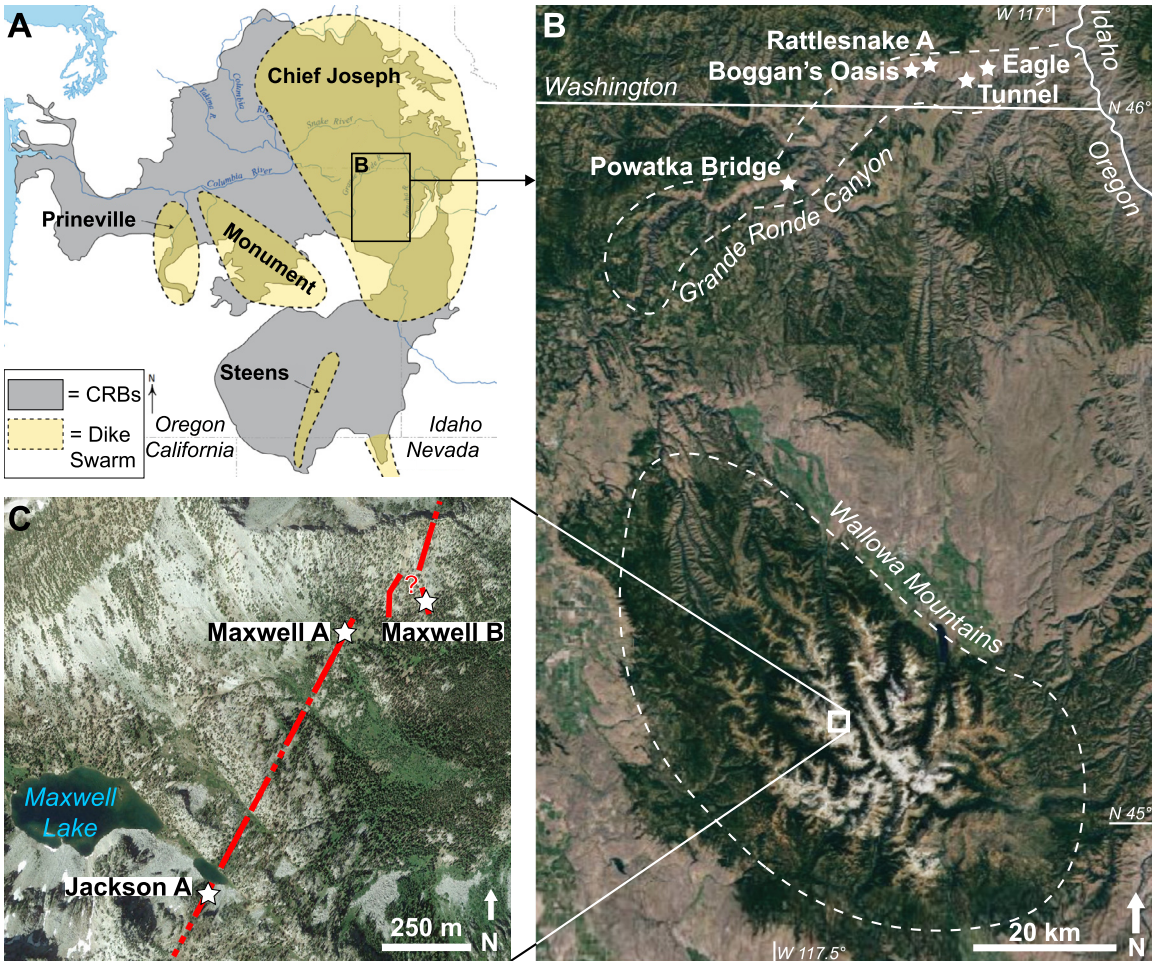

Fig. 1. A) Map of the Columbia River Basalts and associated dike swarms. Lightly modified from Camp et al. (2017). **B)** Satellite image showing the locations of studied dikes in the Grande Ronde Canyon (hosted in earlier CRB flows) and the location of the Wallowa Mountains. **C)** Satellite image of the Maxwell Lake area, showing the locations of three sampled dike segments (hosted in granitoid) that are likely related to the Wapshilla Ridge member of the CRB. Solid lines show where the dikes have been observed, dashed lines show where the dikes are covered. Imagery from Google Earth.

Thordarson and Self, 1998). Other studies, based on analysis of inter-mixing flows (e.g. Reidel, 1998), have suggested that eruptions persist for only a few months. The lavas in the CRB are often crystal-poor (Reidel et al., 2013), so geospeedometry, geothermometry, and cosmogenic surface exposure techniques are difficult to apply here.

All of the dikes sampled in this study are part of the Chief Joseph dike swarm (Fig. 1a), the largest of five dike swarms in the CRB (Taubeneck, 1970; Morriss et al., 2020). Within the Chief Joseph dike swarm we focused on sampling in two areas, the Grande Ronde Canyon (Fig. 1b) and the Cretaceous Wallowa Mountains (Fig. 1b), specifically around Maxwell Lake (Fig. 1c). The highest density of exposed CRB dikes is found in the Cretaceous Wallowa Mountains. In particular, dikes near Maxwell Lake (Fig. 1c) have been the subject of previous studies (Petcovic and Grunder, 2003; Karlstrom et al., 2019; Bindeman et al., 2020). Much of the overlying CRB flows in the Wallowa Mountains have been eroded away so the true paleodepths of the dikes are not known, but Petcovic and Dufek (2005) argue that depths could be as great as 2.5 km. Perry-Houts et al. (2020), based on structure contour mapping of the CRB basal contact, refine the paleodepth of Maxwell Lake area (Fig. 1c) to at least ~400 m, so we estimate a total paleodepth (including ~1 km of prior Imnaha basalts) of ~1.5 km. Dikes in the Grande Ronde river canyon (Fig. 1b) have basaltic wall-rock consisting of earlier CRB flows and generally represent <1 km paleodepths (Table 1).

3. Methods

3.1. Sample collection

We attempted to sample the longest-lived dike segments by targeting feeder dikes to the Wapshilla Ridge member of the CRB, which is among the largest single volcanic units in the world (40,000 km^3, Reidel et al. (2013)). At least two of our dike segments feed this unit (Maxwell A and Jackson A, Table 1). These segments are rimmed by 2–5 m of wall-rock partial melt on either side (Fig. 2a), a rarity in the Chief Joseph dike swarm (only ~3% of Chief Joseph dikes bear outcrop scale evidence for partial melting of host rocks; Morriss et al. (2020)). The combination of these attributes suggest that these segments represent some of the longest total durations of magma transport that the CRB have to offer. We also targeted dikes with clear physical connections to surface flows (Fig. 2b, 2c), to constrain the range of variability in established feeders to surface eruptions.

We collected geochemical and paleomagnetic samples from eight dike segments of the Chief Joseph dike swarm (Tables 1, S1) (Taubeneck, 1970). Studied segments span a range of thicknesses from 2–20 m (the average thickness of Chief Joseph dikes is ~8 m; Morriss et al., 2020). At each site, one or more sampling transects were performed across the dike and surrounding wall-rock (Fig. 2a). Paleomagnetic cores were collected using a handheld electric drill at all of the Grande Ronde Canyon dike

Table 1
Summary of dike properties and geochemistry.

Dike name	Latitude[a]	Longitude[a]	Strike	Dip	Dike width (m)	Paleodepth (m)	Host rock	Partial melt?	Quenched zones?	Affiliation
Jackson A	45.25091	−117.40853	030	68 E	9.0	>1280	Granitoid	Yes	No	Wapshilla Ridge?
Maxwell A	45.25799	−117.40326	030	75 W	8.0	>1400	Granitoid	Yes	No	Wapshilla Ridge
Maxwell B	45.25896	−117.40026	332	80 E	9.5	>1425	Granitoid	No	Margin	Wapshilla Ridge
Tunnel	46.02878	−117.16166	354	~90	19.5	940	CRB Lavas	No	Margin	Umatilla/Sillusi
Powatka Bridge	45.89931	−117.48303	345	~90	20.0	520	CRB Lavas	No	Margin & internal	Elephant Mountain
Rattlesnake A	46.05049	−117.23890	342	~90	2.0	300	CRB Lavas	No	Margin	Roza
Eagle	46.04171	−117.13275	345	~90	7.6	900	CRB Lavas	No	Margin	Buford
Boggan's Oasis	46.04456	−117.25452	336	~90	6.5	340	CRB Lavas	No	Margin & internal	Sentinel Bluffs - Museum

[a] WGS84 Datum.

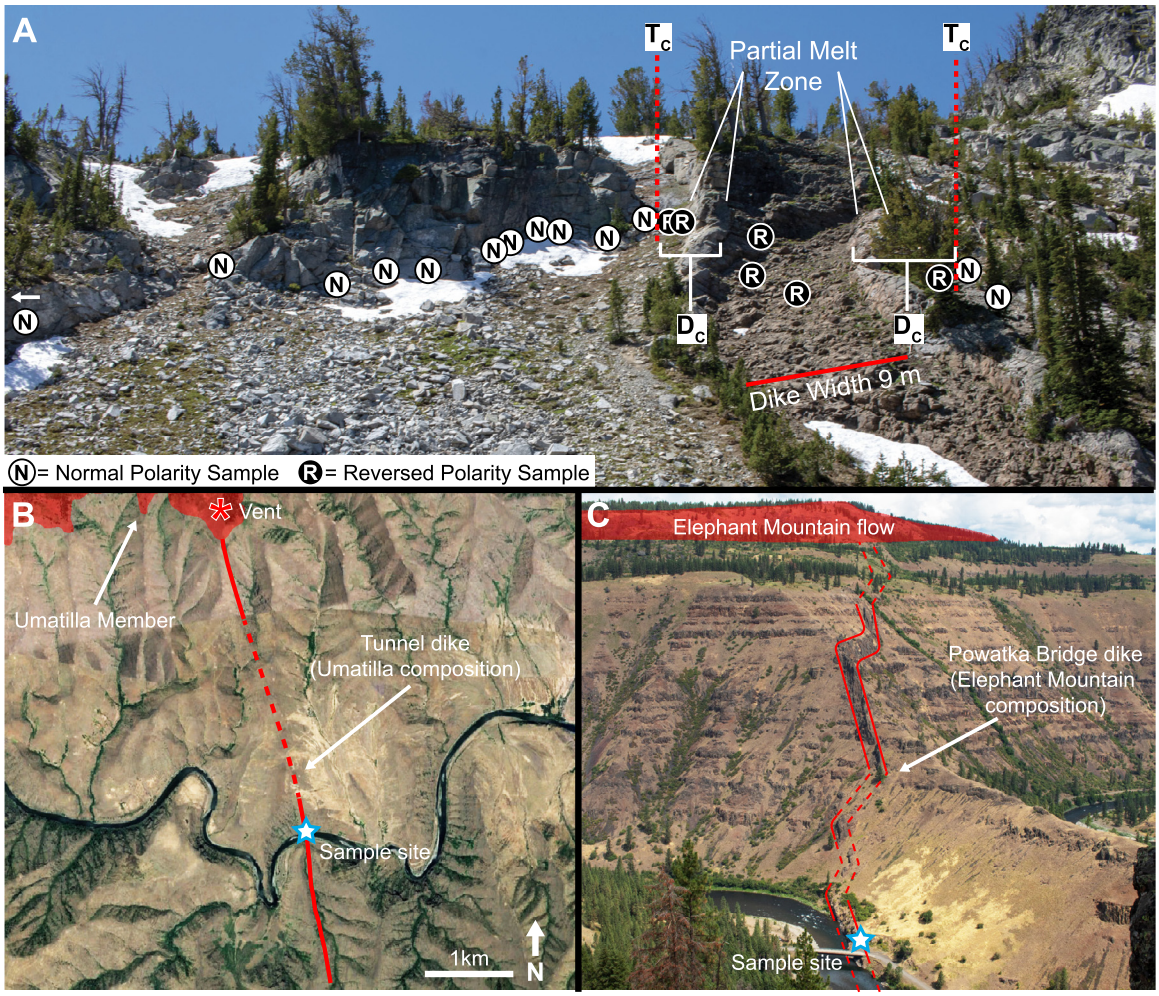

Fig. 2. A) Sampling locations and results from the Jackson A Dike, looking southwest. T_c = location of Curie temperature isotherms, D_c = distance between Curie temperature isotherms and dike margins. Wall-rock samples outside the T_c isotherms retain some of their primary magnetic direction (normal), whereas those between the isotherms are thermally reset and their paleomagnetic direction now matches that of the dike (reversed). **B)** Map of the Tunnel dike (dashed where approximate) and associated vent. The dike has an identical composition to the Umatilla member of the CRB, which is shown in red. Imagery from Google Earth. **C)** Photo of the Powatka Bridge dike (outlined in red, dashed where approximate), looking northwest. The Elephant Mountain member of the CRB, which has an identical composition to the dike, is shown in red. (For interpretation of the colors in the figure(s), the reader is referred to the web version of this article.)

segments (Fig. 1b). These cores were oriented using a Pomeroy orientation device and sun compass measurements when possible. Oriented block samples were collected at the Maxwell Lake segments (Fig. 1c) due to their location in a wilderness area. Sun compass measurements were used to orient the blocks when possible. Any large gaps in block sampling profiles are likely due to a lack of sampleable outcrop. Each block was taken back to the lab and two or more cores (2.54 cm diameter) were drilled into each sample when large enough. Some samples were too small to drill multiple cores while still preserving the orientation markings (e.g. JKA 4, Table S3). Specimens were cut from each core, which were typically 0.5–1 cm in height and 2.54 cm in diameter. Declination corrections were calculated using sun compass measurements when available or using the NOAA geomagnetic field calculator.

3.2. Rock magnetism

To determine the magnetic mineralogy of the samples, thermal-susceptibility curves were measured from representative specimens. These data are also used to determine the Curie temper-

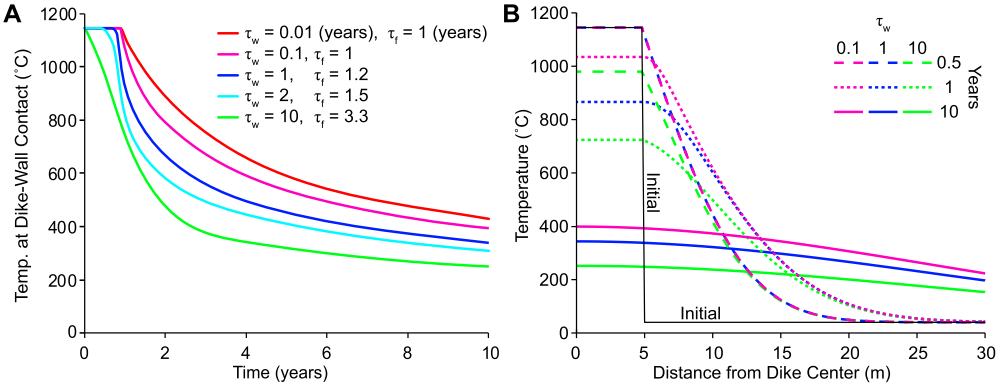

Fig. 3. Effects of flow unsteadiness parameter τ_w on modeled thermal history for fixed flow duration parameter $\tau_c = 1$ year. **A)** Temperature at the dike/wall-rock contact over time. τ_f = dike active lifetime. Note that the total dike lifetime τ_f increases with τ_w but the duration of high-temperature heating at the dike margin decreases. **B)** Temperature vs. distance from the center of the dike after 6 months, 1 year, and 10 years. Base conditions are: far-field background temperature = 40°C, dike width = 10 m, thermal conductivity = 3 $\mathrm{W\,m^{-1}\,K^{-1}}$.

atures (T_c) of the samples, which are necessary for the thermal modeling (see Section 3.4.1). Measurements of thermal-susceptibility curves were performed using an AGICO Multi-Function Kappabridge instrument. The samples were heated from room temperature at a rate of 9 °C/minute, at an operating frequency of 976 Hz, and field intensity of 200 $\mathrm{A\,m^{-1}}$. Maximum temperatures reached were 700 °C, and all experiments were run in an argon atmosphere to minimize oxidation effects. Background 'noise' was removed via the subtraction of a blank sample (run under identical conditions) using AGICO's *Cureval* software.

3.3. Demagnetization

All paleomagnetic samples were measured on a 2G Enterprises vertical SQUID magnetometer with RAPID automatic sample changer at the California Institute of Technology (Kirschvink et al., 2008). The magnetometer is housed in a shielded room with a background field of ~200 nT. Samples at some sites were subject to 20-step thermal demagnetization (100–600 °C), while other samples were subject to 20-step alternating field demagnetization (1.6–90 mT). Some samples were also subjected to two rounds of liquid nitrogen immersion after measurement of NRM in order to enhance the signal of finer (single domain) magnetite grains (Dunlop, 2003), followed by either AF or thermal demagnetization. Characteristic remanence directions were very similar regardless of demagnetization technique. Sample analysis was done using the DemagGUI program as part of the PmagPy software package (Tauxe et al., 2016). Principal component analysis (floating best-fit lines, no origin) was used to determine best-fit directions (Kirschvink, 1980). Maximum angle of deviation (MAD) is reported to assess goodness of fit (Kirschvink, 1980). Best-fits with >16° MAD were excluded from further analysis. Detailed sample statistics are reported with each transect in Table S3.

3.4. Magnetic geothermometer (MGT)

To estimate the total amount of time that each dike segment was transporting magma (hereafter called the intrusion 'lifetime'), we combine two established and complementary techniques described below.

3.4.1. Baked contact test

First, samples from an intrusion and surrounding wall-rock are used for a *baked contact test*. This paleomagnetic technique is used to identify thermal overprinting and resetting of paleomagnetic data in the wall-rock near an igneous intrusion (Graham, 1949; Collinson, 1983). The test can be used to determine which samples have exceeded their Curie temperature (T_c) or blocking temperature (T_b). Samples that are heated above T_c are magnetically 'reset' and the direction of their remanent magnetism will match that of the dike (Fig. 2a). Samples that remained below T_c and T_b will retain their original paleomagnetic direction, though a portion of their magnetization may be altered to match that of the dike (Dunlop and Özdemir, 1997). Crucially, the transfer of heat from dike to wall-rock is a time-dependent process; short-lived intrusions will reset a small volume of wall-rock compared to long-lived intrusions. Here we construct a conservative upper limit to the duration of wall-rock heating by assuming that resetting occurs at 580 °C (T_c of pure elongate magnetite grains) for all samples. Our rock-magnetic data (Fig. S9) suggests that this is a reasonable assumption; see Section 4.2 for further details.

3.4.2. Thermal modeling

Next, we model the heating of wall-rock by a dike, in order to interpret the distance between a dike margin and effective T_c isotherm (hereafter called the Curie distance or D_c, Fig. 2a) in terms of active magma transport that provides a transient heat source. In this study, we use a one-dimensional multi-component thermal conduction and melting model implemented by Karlstrom et al. (2019) (Fig. 3), which simulates continuous magmatic flow through a dike followed by cooling in-place. Several simplifying assumptions are made in this model, some of which are discussed below. Additional model information may be found in Section S5.

Flow of magma is parameterized by a time-evolving dike/host rock contact temperature. While active, the interior temperature $T_d(t)$ of the dike up to the contact is assumed to be spatially uniform but unsteady in time t (up to a total active duration τ_f) according to

$$T_d\left(t < \tau_f\right) = \frac{T_l - T_{bdy}(t)}{2}\left(1 - \tanh\left[10\frac{(t-\tau_c)}{\tau_w}\right]\right) + T_{bdy}(t). \quad (1)$$

Here T_l is the liquidus of the basalt within the dike, and $T_{bdy}(t)$ is the temperature of the host rocks at the dike contact, which evolves in time as conduction proceeds and host rocks heat up. The vigor of actively flowing magma is parameterized by two timescales in Equation (1)—the parameter τ_c is a measure of flow duration, while τ_w models a monotonic decrease of dike boundary temperature as might occur during declining flow. The total duration of dike flow (the 'dike lifetime') τ_f is defined to be the time at which $(T_d(t) - T_{bdy}(0))/(T_l - T_{bdy}(0)) = 0.01$, and is a linear combination of τ_c and τ_w (Fig. 3).

The impact of these timescales on the dike-contact thermal history and subsequent wall-rock time-temperature paths is illustrated in Fig. 3, varying τ_w at constant τ_c. As demonstrated by detailed studies of advection and conduction within a dike (e.g. Petcovic and Dufek, 2005), progressive cooling and associated decline of flow within a dike involves the growth of thermal boundary layers within the dike (and eventually freezing of magma) that cause the hot and near-isothermal core of the dike to retreat from the dike margins in time. Our kinematic approach avoids explicit treatment of unsteady flow within the dike, and thus cannot uniquely resolve contributions to dike margin temperature from viscous dissipation versus driving pressure gradients in the flowing magma (e.g. Fialko and Rubin, 1999). However, with only two parameters, we can effectively explore both the overall timescale of dike flow and the role of flow transience to match thermal constraints from wall-rocks that encompass a range of magma transport scenarios.

A grid search over model parameters constrains the range of possible dike segment lifetimes. Time-temperature histories recorded by D_c are sensitive to a range of parameters including background temperature of the crust, thermal conductivity, and composition-dependent melting of host and dike material (Karlstrom et al., 2019). However, given the large contrast between T_c and initial temperatures of near-surface wall-rocks and the relatively small thermal mass of dikes, the parameters that most strongly affect D_c are those that control the duration of heating by the dike by magma flow. These parameters, τ_c and τ_w, trade off with thermal conductivity of host rocks (Fig. S29) to control D_c, while dike widths or paleodepths in the range of CRB dike exposures (2–10 m widths and 0–2 km depths; Table 1) are not significant. In the case of a flow fed by a single feeder dike, the lifetime of the dike corresponds to the total duration of the eruption itself. Conversely, if a dike exhibits non-monotonic flow the lifetime will be a time-integrated measure of the dike's thermal footprint on host rocks, and thus likely an upper bound on eruption duration. In either case, τ_f cannot distinguish between horizontal versus vertical flow, and thus is an upper bound on eruption duration.

3.4.3. MGT summary

To summarize, the MGT technique combines the baked contact test (Fig. 2a) with a thermal model of the intrusion (Fig. 3). Thermal models have previously been applied to baked contact tests (e.g. Buchan et al., 1980; Kristjansson, 1985), and to planetary thermoremanent magnetization (e.g., Lillis et al., 2009), but overall this approach has been under-utilized given its applicability to most igneous systems. MGT works equally well on young (<1 Ma) and old (e.g., Ga) magmatic systems, as it relies on thermal effects as opposed to radioactive decay. In addition, MGT can also be applied to any host rock containing magnetic minerals that have not been significantly altered or reset since time of reheating.

3.5. Geochemistry

The link between dike segments and lava flows is established on the basis of composition, as physical connections between subsurface transport structures and eruptive deposits are rare in the CRB (Camp et al., 2017). Major oxide and minor element abundances were determined for 15 samples by X-ray fluorescence spectrometry (Table S1). All samples were analyzed using a Panalytical Zetium XRF system at the California Institute of Technology. Major and minor elements were analyzed using fused-glass beads. Following loss on ignition (LOI) determined at 1050 °C, samples were mixed with 9 times their weight in 66.67% $Li_2B_4O_7$–32.83% $LiBO_2$–0.50% LiI flux and fused at 1200 °C.

Unit assignments are based on magnetic polarity (this study, Camp et al., 2017), geologic maps (e.g. Reidel et al., 1992), least-squares regressions to previously published average geochemical compositions of CRB members (Reidel et al., 1992, 2013; Hooper, 2000; Reidel and Tolan, 2013), and mapped extent of CRB members (e.g. Reidel and Tolan, 2013). See Section S1 of the Supplementary Material for more information.

4. Results

4.1. Dike observations and chemistry

A brief summary of observations from each dike segment is below, and more detailed descriptions of each outcrop, including field photos, are available in Section S2. We note that four out of eight dike segments studied here are not found in the extensive Chief Joseph dike swarm maps generated by William H. Taubeneck (Morriss et al., 2020).

The Jackson A dike segment features a ∼2.5 m wide partial melt zone in the wall-rock on either side, which is marked by weathering-resistant granitoid in Fig. 2a and Figure S1. Geochemical data from this segment (Table S1) do not match any published average CRB member compositions, which may be due to assimilation of partially melted wall-rock. Two sampling transects were done here, on either side of the dike (Figs. 2a, S1). Disconnected dike outcrops can be followed along-strike to the Maxwell A segment (Fig. 1c). These segments are thus likely part of the same structural dike system. The western margin of the Maxwell A dike segment features a 2–5 m thick partial melt zone in the wall-rock (granitoid, Fig. S2). The eastern margin is poorly exposed due to erosion. The composition of Maxwell A (Table S1) matches the Wapshilla Ridge member of the CRB, which is the largest member by volume (40,000 km^3).

The Maxwell B dike segment is ∼250 m from the Maxwell A dike (Fig. 1c) and several other segments are present in this hillside (all hosted in granitoid, Fig. S3). A composition reported in Table S1 suggests that this segment is associated with the Wapshilla Ridge member as well. Given the similarities in composition and the close proximity of the Maxwell A and B segments, we hypothesize that they were part of the same magmatic event. Unlike other dike segments in this area, Maxwell B does not feature an obvious partial melt zone in the wall-rock at outcrop scale.

The Tunnel dike (Fig. 2b) is hosted in earlier CRB flows, and three sampling transects were done at this segment—one in a flow interior on the western side, one in a flow interior on the eastern side, and one in a vesicular flow top on the eastern side (Fig. S4). The composition of this segment matches the Umatilla Member of the CRB (720 km^3, Table S1) (Reidel et al., 2013).

The Powatka Bridge dike (Figs. 1b, 2c, S5) is hosted in earlier CRB flows, has several internal quenched margins, and is likely composite with an unknown number of events (Ross, 1983). Therefore, our results capture an integrated thermal history of the dike segment. This might represent the oldest portion if re-injections happened in the middle of the dike, although there is no evidence that this temporal stratigraphy is robust (and indeed, asymmetries in D_c seen at other dikes could be explained by multiple injections that are not centered). We assume that the lifetime reported in Table 2 represents the duration of a single diking event. Although the vent that is fed by this dike is not preserved, the Elephant Mountain member immediately overlies the dike (Fig. 2c) and it can be assumed that this dike breached the paleosurface. The composition of this dike segment matches the Elephant Mountain member of the CRB (440 km^3) (Reidel et al., 2013).

The Rattlesnake A dike (Fig. 1b) is part of a swarm of subparallel dike segments related to the Roza member of the CRB (Thordarson and Self, 1998). Roughly a dozen other Roza segments (all hosted in earlier CRB flows) have been found within 0.5 km of

Table 2
Summary of paleomagnetic and MGT results from CRB Dikes. Distance is measured from the nearest dike margin, second transect is on the footwall side. 'Lifetime' refers to the total duration of magma transport in the dike.

Dike Name	Dike polarity	Wall polarity	D_c (m)[b]	D_c, 2nd transect (m)	MGT-determined lifetime
Jackson A	Reversed	Normal	3.7–5.4	5.6–7.4	0.8–5.0 years
Maxwell A	Reversed	Normal	5.8–8.5	–	0.9–5.6 years
Maxwell B	Reversed	Normal	0–1.15	–	<0.5 years
Tunnel	Normal	Reversed	0.60–0.66	0.18–0.26	0.3–1.3 months
Powatka Bridge	Transitional	Normal	0–0.23	–	<1.1 months
Rattlesnake A[a]	Reversed	Reversed	0–0.20	–	<0.5 months[a]
Eagle[a]	Reversed	Reversed	0–0.65	0–0.28	<1.4 months[a]
Boggan's Oasis[a]	Normal	Normal?	Unclear	–	–

[a] Both dike and wall-rock are the same polarity, see section 4.5.
[b] Distance between the dike margin and T_c 'isotherm'.

this site (Fig. S6). The Rattlesnake A segment is only ~2 m wide, and probably not a major contributor to Roza magma transport.

The Eagle dike (Fig. 1b) appears to be a single-injection event with a jointed core and finely fractured (quenched) margins (Fig. S7). All compositions reported from the core and margins of this segment match the Buford member (Table S1) (Reidel et al., 1992). This dike is hosted in earlier CRB flows.

Finally, the Boggan's Oasis dike (Fig. 1b) also has a jointed core and finely fractured margins, with no internal quenched zones, suggesting a single injection event. This dike is hosted in earlier CRB flows (Fig. S8), and its chemistry suggests an association with the Museum flow of the Sentinel Bluffs member (2349 km^3, see Section S1).

4.2. Rock magnetism

Thermal-susceptibility data show that most wall-rock samples have a T_c of 570–580 °C (Table S2). Some thermal-susceptibility curves show evidence for one pure magnetite phase (Fig. S9a), while others show evidence for multiple phases with multiple Curie temperatures (Fig. S9c). When applying the MGT technique, the highest T_c that is measured in the sample is of greatest importance. Previous studies have found that Curie temperatures can be affected by prior thermal histories such as heating by a dike (e.g. Bowles et al., 2013). However, samples typically have lower T_c *after* heating. A double-heating experiment (Fig. S9d) shows the permanent effects of sample heating on the measured T_c. Since most of our samples still have a T_c near 580 °C, we conclude that these samples did not experience significant lowering of T_c due to dike heating, and therefore assume a T_c of 580 °C is reasonable for all sites in our thermal models. Sensitivity tests with $T_c = 570$ and 550 °C suggest that variable Curie temperatures will lead to estimated dike lifetime differences of <8% (Fig. S31). Thermal-susceptibility curves from dike samples (Table S2) and granitoid wall-rock samples (Fig. S9a, S9b) are mostly reversible. Curves from basaltic wall-rock samples show high variability, with some reversible samples (Fig. S9c) and some that show irreversibility (Fig. S9d), suggesting that alteration or annealing during heating occurred during the experiment.

4.3. Paleomagnetic directions

The Jackson A dike and wall-rock within the resetting zone preserve a reversed magnetic polarity (Fig. 4a, 4b). We found a D_c of 3.7–5.4 m and 5.6–7.4 m from the hanging wall and footwall sides of the dike, respectively (Table 2). Wall-rock samples that are outside of the resetting zone are very poor recorders of paleomagnetic direction. We have plotted best-fit lines in Fig. 4b when possible, but these are not primary thermal remanent magnetization directions from the cooling of the granodiorite batholith. Instead, they are likely recording the modern paleomagnetic field direction via a weak viscous remanent magnetization (Yu and Tauxe, 2006).

The Maxwell A dike and wall-rock within the resetting zone also preserve a reversed magnetic polarity (Fig. 4c, 4d). We found a D_c of 5.8–8.5 m (Table 2), and only one wall-rock sample was not reset (MXA 5).

The Maxwell B dike preserves a reversed magnetic polarity, while the wall-rock samples only have a viscous remanent magnetization (Fig. 4e, 4f). In this case, the closest wall-rock sample (1.15 m from the dike margin) was not reset, so there is no firm lower bound on the MGT-determined lifetime at this exposure (Table 2). Primary remanence directions from the Maxwell A and B dikes are both reversed, but notably different (Fig. 4d, 4f). This suggests that the Maxwell B dike may represent a different Wapshilla Ridge flow than Maxwell A or Jackson A, as this CRB member is composed of >18 flows that are geochemically similar (Reidel and Tolan, 2013).

At the Tunnel Dike (Fig. 1b), the dike and wall-rock within the resetting zone preserve a normal magnetic polarity (Figs. 4g, 4h, S16). Wall-rock samples that are outside of the resetting zone preserve a reversed magnetic polarity. On the western side, D_c is well constrained to 60–66 cm from the dike margin (Table 2). On the eastern (footwall) side D_c is 18–30 cm in the flow interior and 18–26 cm in the flow top. We expect fluid flow and circulation to be more prevalent in the vesicular flow top, but our results suggest that this did not have a significant impact on D_c.

The Powatka Bridge dike preserves a transitional magnetic polarity (Fig. 4i, 4j), which is in agreement with previous measurements from the Elephant Mountain member (Choiniere and Swanson, 1979). Wall-rock samples preserve a normal magnetic polarity. None of the wall-rock samples were reset by the dike, so the MGT-determined lifetime reported in Table 2 does not have a firm lower bound.

The Rattlesnake A dike preserves a reversed direction, and wall-rock samples also preserve a reversed magnetic polarity (Fig. 5a, 5b). In this case it is not initially clear if any wall-rock samples have been reset by the dike, but several lines of evidence suggest that extensive resetting has not occurred here. The average dike direction is $D = 189.6$, $I = -56.9$, $a95 = 15.1$, $N = 3$, while the average wall-rock direction is $D = 168.8$, $I = -42.1$, $a95 = 5.3$, $N = 12$. The test of mean directions (Fisher et al., 1993) can be applied to these averages to determine their degree of similarity. Applying the test yields a 99.99% confidence that the dike and wall-rock mean directions are different. See Section 4.5 for further discussion.

The magnetization preserved in the Eagle is complex (likely due to a nearby lightning strike, Fig. 5c, 5d), and a discussion of these results is included in Section S4.7. We conclude that both the dike and wall-rock samples preserve a reversed magnetic polarity. Again it is not initially clear if any wall-rock samples have been reset by the dike, but several lines of evidence suggest that extensive re-

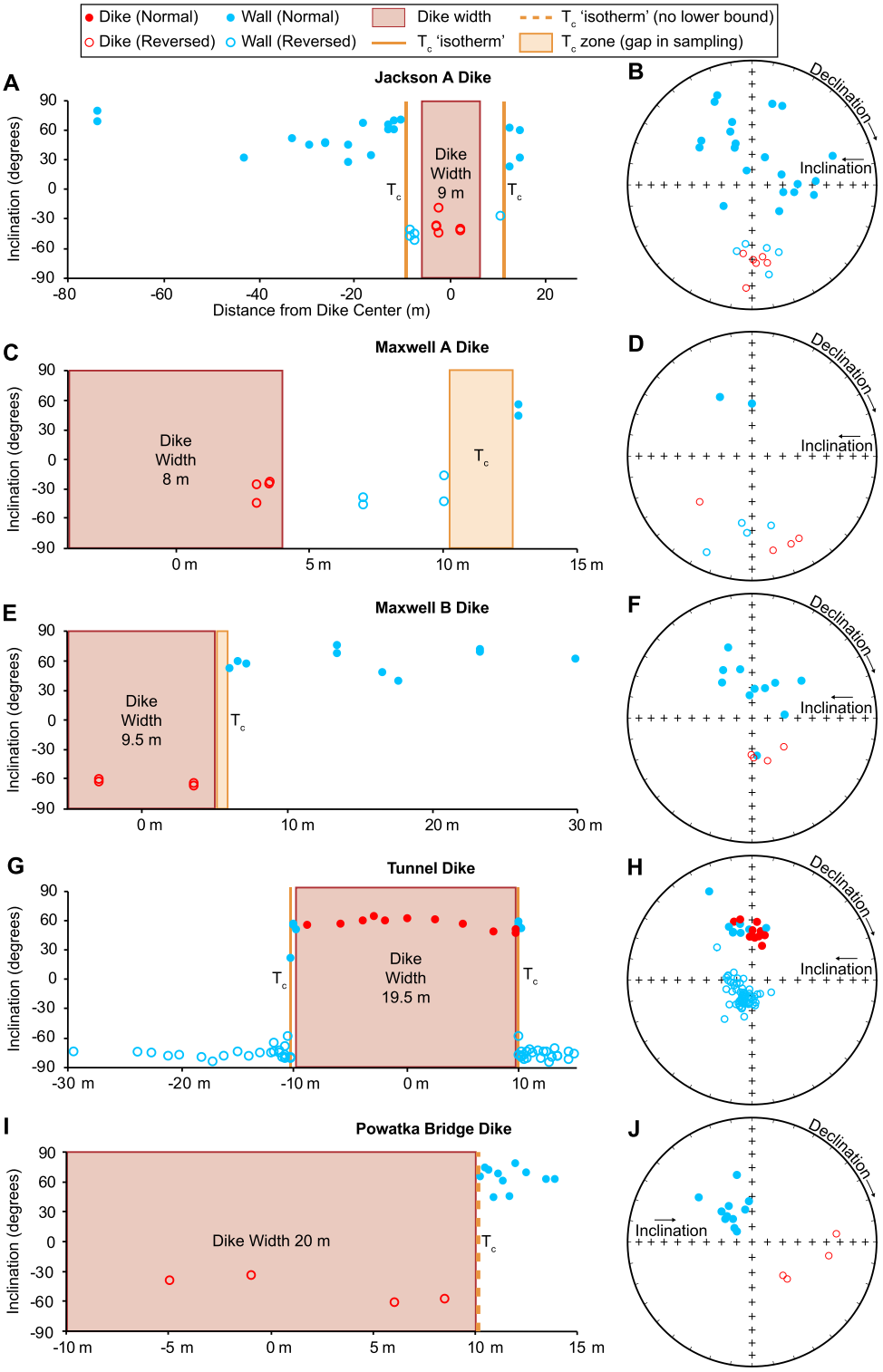

Fig. 4. Paleomagnetic results from five CRB dike segments where the dike and wall-rock have different polarities. **Left column)** Distance from the dike center (x-axis) vs. inclination of the primary paleomagnetic remanence (y-axis). T_c = Curie temperature 'isotherm'. **Right column)** Equal area projection showing primary remanence directions for each dike segment.

setting has not occurred here either. The average (reversed) dike direction is $D = 218.8$, $I = -46.5$, $a95 = 11.8$, $N = 5$, while the average wall-rock direction is $D = 216.6$, $I = -55.3$, $a95 = 1.9$, $N = 23$. Applying the test of mean directions (Fisher et al., 1993) to these data yields a 91.7% confidence that the dike and wall-rock mean directions are different. See Section 4.5 for further discussion.

Finally, at the Boggan's Oasis dike, the wall-rock and dike directions show significant scatter (Fig. 5e, 5f). Given the scattered nature of these data, we conclude that the MGT technique cannot be applied in this instance. For example, the closest sample (BD2 6, Table S3) is 5 cm from the dike margin and would be reset regardless of dike lifetime. However, this resetting is not clearly evident in the highly scattered data from this dike (Fig. 5f).

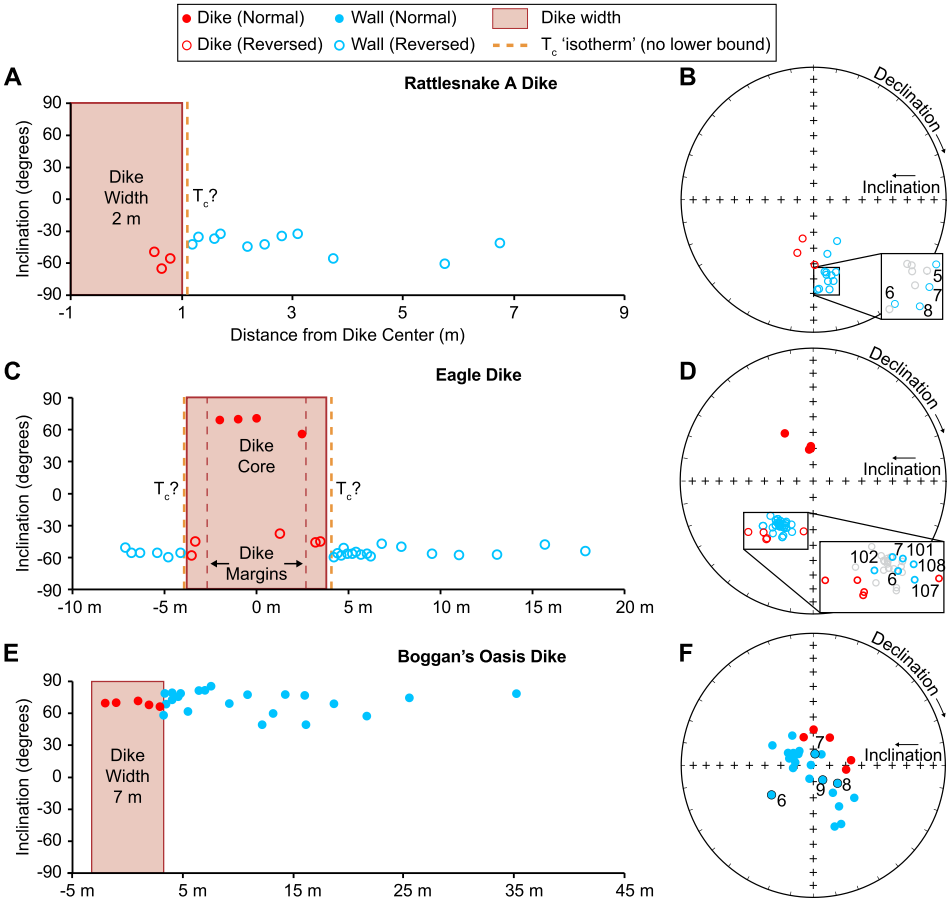

Fig. 5. Paleomagnetic results from three CRB dike segments where the dike and wall-rock have the same polarity. **Left column)** Distance from the dike center (x-axis) vs. inclination of the primary paleomagnetic remanence (y-axis). T_c = Curie temperature 'isotherm'. **Right column)** Equal area projection showing primary remanence directions for each dike segment. Insets show wall-rock samples within 1 m of the dike in blue (with sample numbers, see Table S3), while more distant wall-rock samples are in grey. See Sections 4.3 and 4.5 for discussion.

4.4. Magnetic geothermometer

After conducting baked contact tests, the thermal model can now be used to determine which range of dike lifetimes will produce the measured D_c (Fig. 6 and Table 2). Where possible, we have defined D_c on both sides of a given dike segment. Dike segment lifetimes range from 0–6 years, but these lifetimes are not distributed evenly between the sites. All four dikes in the Grande Ronde Canyon (Fig. 1b) show relatively short lifetimes of $\lesssim$ 1 year (Fig. 6a). At four dike segments (Maxwell B, Powatka Bridge, Rattlesnake A, and Eagle) the closest samples to the dike were not reset, so there is no lower bound on the MGT-determined lifetimes (Fig. 6a; Table 2).

Two dike segments in the Maxwell lake area (Jackson A and Maxwell A; Fig. 1c) show relatively long lifetimes of 1–6 years (Fig. 6a; Table 2), which is expected given the zones of partially melted wall-rock surrounding these segments (Fig. 2a). This range of uncertainty is primarily controlled by the relative proportion of flow unsteadiness τ_w to active lifetime in the thermal model (Fig. 3, 6a). While flow duration and unsteadiness can vary between dike segments, the efficacy of heat transport through wall-rocks is not expected to vary greatly between nearby dike segments. The Maxwell A and Maxwell B segments are ~250 meters from each other (Figs. 1c, S3) and hosted in granodiorite with minimal macroscopic fracture density at the same paleodepth. This same logic applies to the studied dike segments within basaltic host rock (Fig. 1b). Thermal conductivity and degree of fluid-mediated heat transport might in principle vary between sites, as articulated by an ongoing debate about the general role of meteoric fluids in alteration of CRB rocks (Sawlan, 2017; Baker et al., 2019). However, variations in active magma flow are the simplest and hence most plausible way to account for the high temperature variation seen in D_c from our data. The trade-offs between these variables are shown in Fig. 3.

4.5. Non-ideal results

Two sites have a reversed magnetic polarity in both the wall-rock and dike (Figs. 5b, 5d). This makes it more difficult to determine which wall-rock samples have been reset by the dike. At the Rattlesnake A dike (Fig. 5b), resetting of all wall-rock samples would require an unrealistic dike lifetime of 1–4.3 years, which is inconsistent with field observations of this dike segment (quenched margins, no partial melt in wall-rock). Given that the Rattlesnake A segment is one of dozens in the Roza dike swarm (Fig. S6; Thordarson and Self, 1998), this narrow dike segment was probably not a long-lived principal feeder segment to the Roza member. The inset portion of Fig. 5b shows that wall-rock samples within 1 m of the dike margin (5, 6, 7, and 8) are not systematically similar in direction to the dike samples. Together, this evidence (along with the test of mean directions, Section 4.3) suggests that no samples were reset. Nevertheless, the MGT-determined lifetime reported in Table 2 is less certain than the lifetimes of other dikes. See the section S4.6 for additional information.

At the Eagle dike (Fig. 5d), resetting of all wall-rock samples is effectively impossible as it would require a dike lifetime of >10 years, which is inconsistent with field observations of this dike segment (quenched margins, no partially melted wall-rock). The

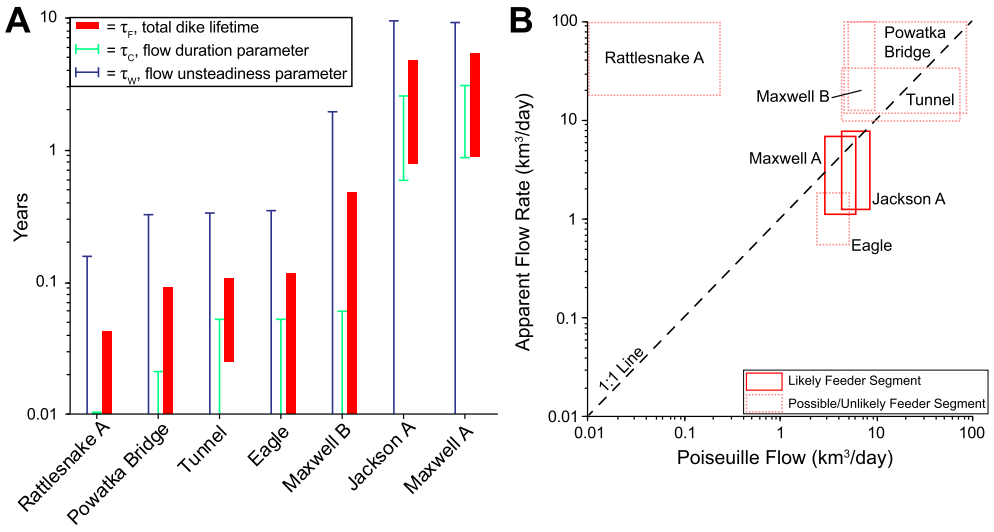

Fig. 6. A) MGT results from seven dike segments in this study, showing a bimodal distribution of dike lifetimes (red bars). Blue and green lines indicate the range of uncertainty for each flow parameter in Equation (1) as determined by a grid search through τ_c and τ_w (Fig. S30). **B)** Results from apparent flow rate calculations (y-axis, Table 3) plotted against the expected flow rates from Poiseuille flow calculations using outcrops to estimate dike width (x-axis). Horizontal width of symbol represents uncertainty in active width of the dike (see Table 3). The dashed boxes represent upper bounds for both axes based on the model assumptions. See Section 5.4 for details.

dike feeds one of the smallest CRB members (Buford, 20 km^3) (Reidel et al., 2013) and shows no field evidence for multiple injections. There appears to be no systematic variation in the wall-rock direction, as shown in the inset portion of Fig. 5d, which highlights samples that are within 1 m of the dike margins. The closest wall-rock samples are not systematically similar in direction to the dike samples. This evidence (along with the test of mean directions, Section 4.5) again suggests that no samples were reset. We are less certain of this interpretation at this dike than at Rattlesnake A, and additional data could disprove this assumption, so the MGT-determined lifetime reported in Table 2 is less certain than the lifetimes of the dikes previously discussed.

5. Discussion

5.1. Agreement with previous CRB dike longevity estimates

The MGT results presented in this study are in agreement with previously published results from other methods at our study sites (Fig. 7). Reidel (1998) suggested that the Tunnel dike, and its associated vent, were active for a few months or less based on flow mapping, geochemistry, and thermal arguments. Studies of the Maxwell A dike (Petcovic and Grunder, 2003; Petcovic and Dufek, 2005) modeled geothermometry from partially melted wall-rocks to estimate that the dike segment was active for 3–4 years. (U-Th)/He thermochronology of the Jackson A dike segment suggested an active lifetime of 1.4–5.4 years (at 68% confidence from a Bayesian conduction model inversion; Karlstrom et al., 2019), which matches models for oxygen isotope depletion observed around that segment which accounts for advective fluid-mediated heat transport in wall-rocks (Bindeman et al., 2020). Consistency between MGT and other independent estimates provides confidence in the accuracy of this method when applied to sites that are not amenable to study with the techniques listed above.

5.2. Heterogeneity in dike thermal footprints

The CRB are associated with over four thousand mapped dike segments (Morriss et al., 2020), but it is an open question regarding how many of these segments actively fed flows and for how long. While the eight segments analyzed in this study are not a representative sample of the entire system, they provide an important baseline that illustrates the likely variability in shallow crustal magma transport for the flood basalt province.

Two nearby dikes (Maxwell A and Maxwell B, Fig. 1c) have the same composition (Wapshilla Ridge member, Petcovic and Grunder (2003)). However, these dike segments have different D_c (Table 2), suggesting that segments feeding the same eruptive episode were not active for the same amount of time. A nearby dike (Jackson A) is likely another segment of the same dike as Maxwell A, as they are on-strike with each other and only ∼1 km apart (Fig. 1c). Both segments exhibit evidence for prolonged transport and heating, but differences in the amount of partially melted wall-rock suggest that they may not have been active for the same amount of time either. Based on these observations and our results, we conclude that flow localization resulted in variable durations of magma transport within CRB dikes. Table 2 shows that the studied dike segments have a broad distribution of D_c, with consistent but sometimes asymmetric heating on either side of the dike segment. If multiple injections occurred (e.g. Thiele et al., 2021) they do not need to intrude along the dike centerline, so such non-monotonic thermal histories are one way to explain the slight asymmetries in D_c observed in our data. Alternatively, these asymmetries could be explained by mechanical erosion of the wall-rock contact during magma transport.

5.3. Links to eruption style

MGT results suggest that some dike segments can be active for less than one month (Table 2). Given the large effusive volume of CRB eruptions, this implies a fissure-style eruption characterized by very high eruption rates if the segments with small D_c were active feeders to observed flows (e.g. Fig. 2b, c). However, it is also possible some segments of a given dike were actively erupting over months or years while other segments were essentially inactive. This is a plausible explanation for our variety of MGT results (e.g., the distributions of τ_w and τ_c) and the field evidence for long versus short eruption durations (e.g. Reidel, 1998; Thordarson and Self, 1998). The MGT evidence for closely separated portions of a dike system with dissimilar transport times suggests along-strike localization of flow during the eruption. This behavior, common to historic basaltic fissure eruptions (e.g. Thordarson and Self, 1993),

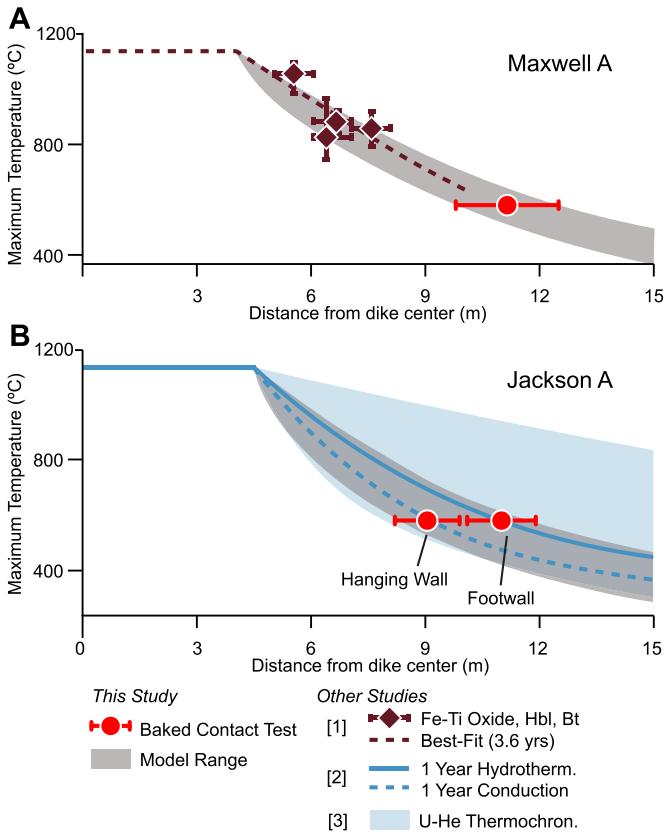

Fig. 7. A) MGT results from the Maxwell A dike (red circles) compared to Fe-Ti oxide, hornblende, and biotite results from [1] Petcovic and Grunder (2003). The range of model solutions from this study that are in agreement paleomagnetic results is shown in grey. **B)** MGT results from the Jackson A dike (red circles). Greater D_c in the footwall side of the dike might arise from the non-planar dike geometry seen in Fig. 2a, or reflect asymmetric heat transport efficacy below versus above the dipping dike structure. [2] Hydrothermal convection and conduction simulations from Bindeman et al. (2020) matching $\delta^{18}O$ depletion profile around the dike. [3] (U-Th)/He thermochronology 68% confidence envelope of $>10^6$ simulations from Karlstrom et al. (2019).

has been explained through thermoviscous focusing (e.g. Wylie et al., 1999) or mechanical erosion associated with wall-rock fracturing (e.g. Delaney and Pollard, 1982).

5.4. Eruption rates

Each dike can be linked to an associated CRB member (Table S1), and the volume and number of flows have been previously estimated for each member (Reidel et al., 2013; Reidel and Tolan, 2013). Assuming that our dike active lifetimes are representative of their associated eruptive units, we can calculate an *apparent* upper bound eruption rate per eruptive unit by dividing CRB member volume by the number of flows and MGT-determined dike lifetime. We use the full range of active lifetimes τ_f for each dike segment to provide rough estimates, with the understanding that variations in boundary temperature implied by variable τ_w reflect time variations in flow rate, Q, (Karlstrom et al., 2019), and unknown partitioning between horizontal and vertical flow. If flow is primarily horizontal, τ_f may not correspond in a simple way with eruption rates. However, the shallow paleodepths of dikes here justify an initial assumption of dominantly vertical flow.

The calculated eruption rates (Table 3, Fig. 6b) are notably high in most cases. We assess their physical plausibility with a calculation of flow rates given known dike segment geometry: Assuming Poiseuille flow through a rectangular slot, Q is a function of segment width w and length L, with dynamic viscosity μ driven by pressure gradient $\frac{dP}{dz}$,

$$Q = \frac{w^3 L}{3\mu}\left|\frac{dP}{dz}\right|. \tag{2}$$

Assuming Q corresponds to the eruption rate determined by MGT, we can independently estimate parameters on the right-hand-side of Equation (2). Active length is poorly constrained, but historical basaltic fissure eruptions (Thordarson and Self, 1993), and rare exposures of CRB vent facies (Brown et al., 2014) suggest that lengths of ~1 km are likely appropriate. Measured whole rock compositions (Table S1) constrain liquidus viscosity (neglecting the effects of water) to be $\leq 10^3$ Pa s (Hui and Zhang, 2007), and buoyancy driven flow implies driving pressure gradients of perhaps several hundred Pa m^{-1} (e.g. Rivalta et al., 2015). The greatest unknown, with cubic dependence in Equation (2), is width of active flow within the dike segment.

If the calculated eruption rate can be reasonably reconciled with the Poiseuille flow model using observed dike segment width (including uncertainty in width as a proxy for error in all parameters), then the segment is deemed a 'likely feeder segment' (Table 3, Fig. 6b). If the calculated eruption rate differs from the Poiseuille flow model, then the segment is deemed an 'unlikely feeder', indicating that our MGT transect happened to intersect a portion of the dike that did not significantly contribute to its associated eruption.

Two MGT profiles (Jackson A and Maxwell A) are self-consistent with preserved structures, implying volumetric eruption rates of 1.1–7.7 $km^3\,day^{-1}$ during eruption of the Wapshilla Ridge member (Fig. 6b, Table 3). This is >10 times the average Laki 1783 fissure eruption rate of ~0.09 $km^3\,day^{-1}$ (Thordarson and Self, 1993). Three segments (Tunnel, Powatka, Eagle) are judged to be 'possible feeders', because some of the MGT-determined eruption rates are self-consistent with preserved structures. Finally, two segments (Maxwell B, Rattlesnake A) are 'unlikely feeders' (Table 3, Fig. 6b) because their MGT-determined eruption rates are not physically possible according to our Poiseuille flow calculations (Fig. 6b)

5.5. Applicability to other flood basalts

This study focuses on the CRB, which is the youngest and smallest flood basalt on Earth. Therefore, the applicability of these results to other flood basalt provinces that had larger total volumes and a larger impact on the global climate and biosphere is not immediately clear. Our maximum eruption rate estimates (1.1–7.7 $km^3\,day^{-1}$) are several orders of magnitude higher than long-term eruption rates calculated for the Deccan Traps (~0.002 $km^3\,day^{-1}$; Schoene et al. (2019), Sprain et al. (2019)), Siberian Traps (~0.009 $km^3\,day^{-1}$; Burgess et al. (2017)), and the CRB (~0.0009 $km^3\,day^{-1}$; Kasbohm and Schoene (2018)). They are more comparable to (although still larger than) previous estimates of individual CRB units, such as the Roza (~0.58 km^3/day; Thordarson and Self, 1998). Since the long-term CRB eruption rate is significantly less than the rates of individual eruptions determined in this study, this suggests activity from LIP-related basaltic volcanism is highly unsteady in time even during prolonged eruptive episodes (Mather and Schmidt, 2021). Although the CRB are smaller than other flood basalts, the volumes of CRB main phase eruptions ($\gtrsim$1000 km^3; Reidel et al. (2013)) are similar to the volumes of Deccan eruptions (Self et al., 2008). The widths of CRB dikes (~8 m on average; Morriss et al. (2020)) are also similar to dikes in the Deccan Traps (Ray et al., 2006). Therefore, we hypothesize that other flood basalt eruptions operate on a similar range of magma transport timescales as described here.

Table 3
Eruption rates and Poiseuille flow calculations. Parameters are: $\mu = 1000$ Pa s, L = 1000 m, $\partial P/\partial z = 300$ Pa m^{-1}.

Dike name	Active width (w) (m)	Total volume (km^3)	# of flows[a,b]	Apparent eruption rate (km^3 day^{-1})	Poiseuille flow rate (km^3 day^{-1})	Conclusion
Jackson A	8–10	40250[a]	18	1.2–7.7	8.6–4.4	Likely feeder segment
Maxwell A	7–9	40250[a]	18	1.1–6.8	6.3–3	Likely feeder segment
Maxwell B	8.5–10.5	40250[a]	18	>12.3	5.3–10	Unlikely feeder segment
Tunnel	8–20.5[c]	720[b]	2	9.9–33	4.4–74	Possible feeder segment
Powatka Bridge	8–21[c]	440[b]	1	>12	4.4–80	Possible feeder segment
Rattlesnake A	1–3	1300[b]	5	>18	0.01–0.2	Unlikely feeder segment[d]
Eagle	6.6–8.6	20[b]	1	>0.5	2.5–5.5	Possible feeder segmant[d]

Data from: Reidel and Tolan (2013)[a], Reidel et al. (2013)[b], [c]Composite dikes are assumed to have a minimum width of 8 m, the CRB average (Morriss et al., 2020), [d]Assuming no wall-rock samples are reset, see Section 4.5.

6. Conclusions

We implemented a magnetic geothermometer for determining timescales of magma transport in igneous intrusions and applied this to eight CRB dike segments that likely fed known lava flows. We found a range of active transport lifetimes from several years to less than one month. Two dikes (Maxwell A and Jackson A) are rimmed by partially melted wall-rock, and likely fed the largest member of the CRB at average rates of 1.1–7.7 km^3 day^{-1}. Our survey also finds segments that did not contribute significantly to associated eruptions, and evidence for composite structures. A resulting picture of the shallow (<2 km depths) CRB plumbing system emerges in which re-use of transport structures that feed surface eruptions and along-strike localization of magma flow are commonplace. Transport durations can vary over short (<1 km) length scales along flood basalt dikes, which is consistent with transitions from fissure-style to conduit-fed eruptions. The implied shortening of individual eruption timescales compared to province-scale emplacement should have significant implications for short-term climatic effects of the CRB and other flood basalt provinces.

The MGT technique employed in this study complements other methods by providing thermal history constraints regardless of host rock composition and age. MGT results can be determined in the lab in a short amount of time and at a low cost. However, the single temperature constraint is somewhat limiting. As with other methods, MGT will provide better constraints when used in combination with other techniques. A clear theoretical advance would be to better understand the kinetics of partial magnetic resetting in titanomagnetites, which would increase the resolving power of MGT for time-temperature histories.

CRediT authorship contribution statement

Joseph Biasi: Conceptualization, Data curation, Formal analysis, Investigation, Methodology, Project administration, Resources, Validation, Visualization, Writing – original draft, Writing – review & editing. **Leif Karlstrom:** Data curation, Funding acquisition, Methodology, Resources, Software, Validation, Writing – review & editing.

Declaration of competing interest

The authors declare that they have no known competing financial interests or personal relationships that could have appeared to influence the work reported in this paper.

Data availability

All paleomagnetic data are available via the MagIC database at https://earthref.org/MagIC/19000. Matlab code required to reproduce thermal modeling results may be downloaded from Github: https://github.com/leifkarlstrom/dike_conductiveheating_1d.

Acknowledgements

The authors wish to thank Samuel Piascik, Marcel Griffioen, and Sydney Acito for their assistance with the project. Matthew Morris is thanked for his digitization of CRB dike data and suggestions for where to sample. The University of Oregon field camp is acknowledged for logistical support. Anita Grunder is thanked for helpful discussions regarding previous work. Joseph Kirschvink is greatly thanked for helpful discussions and use of his paleomagnetic laboratory. This work was supported in part by NSF CAREER 1848554 to LK and a GSA AGeS2 award to JB.

Appendix A. Supplementary material

Supplementary material related to this article can be found online at https://doi.org/10.1016/j.epsl.2021.117169.

References

Baker, L.L., Camp, V.E., Reidel, S.P., Martin, B.S., Ross, M.E., Tolan, T.L., 2019. Alteration, mass analysis, and magmatic compositions of the Sentinel Bluffs Member, Columbia River flood basalt province: comment. Geosphere 15, 1436–1447. https://doi.org/10.1130/GES02047.1.

Bindeman, I., Greber, N., Melnik, O., Artyomova, A., Utkin, I., Karlstrom, L., Colón, D., 2020. Pervasive hydrothermal events associated with large igneous provinces documented by the Columbia River basaltic province. Sci. Rep. 10, 1–9. https://doi.org/10.1038/s41598-020-67226-9.

Bowles, J.A., Jackson, M.J., Berquó, T.S., Sølheid, P.A., Gee, J.S., 2013. Inferred time- and temperature-dependent cation ordering in natural titanomagnetites. Nat. Commun. 4, 1–9.

Brown, R.J., Blake, S., Thordarson, T., Self, S., 2014. Pyroclastic edifices record vigorous lava fountains during the emplacement of a flood basalt flow field, Roza Member, Columbia River Basalt Province, USA. GSA Bull. 126, 875–891. https://doi.org/10.1130/B30857.1.

Buchan, K., Schwarz, E., Symons, D., Stupavsky, M., 1980. Remanent magnetization in the contact zone between Columbia Plateau flows and feeder dikes: evidence for groundwater layer at time of intrusion. J. Geophys. Res., Solid Earth 85, 1888–1898. https://doi.org/10.1029/JB085iB04p01888.

Burgess, S.D., Muirhead, J.D., Bowring, S.A., 2017. Initial pulse of Siberian Traps sills as the trigger of the end-Permian mass extinction. Nat. Commun. 8, 1–6. https://doi.org/10.1038/s41467-017-00083-9.

Camp, V.E., Reidel, S.P., Ross, M.E., Brown, R.J., Self, S., 2017. Field-trip guide to the vents, dikes, stratigraphy, and structure of the Columbia River Basalt Group, eastern Oregon and southeastern Washington, U.S. Geological Survey Scientific Investigations Report USGS Numbered Series 2017-5022-N. 104 p.

Choiniere, S.R., Swanson, D.A., 1979. Magnetostratigraphy and correlation of Miocene basalts of the northern Oregon coast and Columbia Plateau, southeast Washington. Am. J. Sci. 279, 755–777. https://doi.org/10.2475/ajs.279.7.755.

Clapham, M.E., Renne, P.R., 2019. Flood basalts and mass extinctions. Annu. Rev. Earth Planet. Sci. 47, 275–303. https://doi.org/10.1146/annurev-earth-053018-060136.

Collinson, D.W., 1983. Methods in Rock Magnetism and Palaeomagnetism: Techniques and Instrumentation. Chapman and Hall, London, New York. 503 p.

Delaney, P.T., Pollard, D.D., 1982. Solidification of basaltic magma during flow in a dike. Am. J. Sci. 282, 856–885. https://doi.org/10.2475/ajs.282.6.856.

Dunlop, D.J., 2003. Stepwise and continuous low-temperature demagnetization. Geophys. Res. Lett. 30. https://doi.org/10.1029/2003GL017268.

Dunlop, D.J., Özdemir, Ö., 1997. Rock Magnetism: Fundamentals and Frontiers. Cambridge Studies in Magnetism. Cambridge University Press, Cambridge. 573 p.

Fendley, I.M., Mittal, T., Sprain, C.J., Marvin-DiPasquale, M., Tobin, T.S., Renne, P.R., 2019. Constraints on the volume and rate of Deccan Traps flood basalt eruptions using a combination of high-resolution terrestrial mercury records and geochemical box models. Earth Planet. Sci. Lett. 524, 115721.

Fialko, Y.A., Rubin, A.M., 1999. Thermal and mechanical aspects of magma emplacement in giant dike swarms. J. Geophys. Res., Solid Earth 104, 23033–23049. https://doi.org/10.1029/1999JB900213.

Fisher, N.I., Lewis, T., Embleton, B.J., 1993. Statistical Analysis of Spherical Data. Cambridge University Press, Cambridge, UK. 343 p.

Graham, J.W., 1949. The stability and significance of magnetism in sedimentary rocks. J. Geophys. Res. 54, 131–167. https://doi.org/10.1029/JZ054i002p00131.

Hooper, P.R., 2000. Chemical discrimination of Columbia River basalt flows. Geochem. Geophys. Geosyst. 1. https://doi.org/10.1029/2000GC000040.

Hui, H., Zhang, Y., 2007. Toward a general viscosity equation for natural anhydrous and hydrous silicate melts. Geochim. Cosmochim. Acta 71, 403–416. https://doi.org/10.1016/j.gca.2006.09.003.

Karlstrom, L., Murray, K.E., Reiners, P.W., 2019. Bayesian Markov-chain Monte Carlo inversion of low-temperature thermochronology around two 8-10 m wide Columbia River flood basalt dikes. Front. Earth Sci. 7, 90. https://doi.org/10.3389/feart.2019.00090.

Kasbohm, J., Schoene, B., 2018. Rapid eruption of the Columbia River flood basalt and correlation with the mid-Miocene climate optimum. Sci. Adv. 4. https://doi.org/10.1126/sciadv.aat8223.

Kirschvink, J., 1980. The least-squares line and plane and the analysis of palaeomagnetic data. Geophys. J. Int. 62, 699–718. https://doi.org/10.1111/j.1365-246X.1980.tb02601.x.

Kirschvink, J.L., Kopp, R.E., Raub, T.D., Baumgartner, C.T., Holt, J.W., 2008. Rapid, precise, and high-sensitivity acquisition of paleomagnetic and rock-magnetic data: development of a low-noise automatic sample changing system for superconducting rock magnetometers. Geochem. Geophys. Geosyst. 9. https://doi.org/10.1029/2007GC001856.

Kristjansson, L., 1985. Magnetic and thermal effects of dike intrusions in Iceland. J. Geophys. Res., Solid Earth 90, 10129–10135. https://doi.org/10.1029/JB090iB12p10129.

Lillis, R.J., Dufek, J., Bleacher, J.E., Manga, M., 2009. Demagnetization of crust by magmatic intrusion near the Arsia Mons volcano: magnetic and thermal implications for the development of the Tharsis province, Mars. In: Tectonic and Volcanic History of the Tharsis Province, Mars. J. Volcanol. Geotherm. Res. 185, 123–138. https://doi.org/10.1016/j.jvolgeores.2008.12.007.

Mather, T.A., Schmidt, A., 2021. Environmental effects of volcanic volatile fluxes from subaerial large igneous provinces. In: Large Igneous Provinces. American Geophysical Union (AGU), pp. 103–116.

Morriss, M.C., Karlstrom, L., Nasholds, M.W., Wolff, J.A., 2020. The Chief Joseph dike swarm of the Columbia River flood basalts, and the legacy data set of William H. Taubeneck. Geosphere 16, 1082–1106. https://doi.org/10.1130/GES02173.1.

Perry-Houts, J., Schoettle-Greene, P., Humphreys, G., Klema, N., O'Hara, D., Colón, A., 2020. The Columbia River Basalt as a record of Miocene topography and the deformation that followed. In: AGU Fall Meeting 2020. AGU.

Petcovic, H.L., Dufek, J.D., 2005. Modeling magma flow and cooling in dikes: implications for emplacement of Columbia River flood basalts. J. Geophys. Res., Solid Earth 110. https://doi.org/10.1029/2004JB003432.

Petcovic, H., Grunder, A., 2003. Textural and thermal history of partial melting in tonalitic wallrock at the margin of a basalt dike, Wallowa Mountains, Oregon. J. Petrol. 44, 2287–2312. https://doi.org/10.1093/petrology/egg078.

Ray, R., Sheth, H.C., Mallik, J., 2006. Structure and emplacement of the Nandurbar–Dhule mafic dyke swarm, Deccan Traps, and the tectonomagmatic evolution of flood basalts. Bull. Volcanol. 69, 537. https://doi.org/10.1007/s00445-006-0089-y.

Reidel, S.P., 1998. Emplacement of Columbia River flood basalt. J. Geophys. Res., Solid Earth 103, 27393–27410. https://doi.org/10.1029/97JB03671.

Reidel, S.P., Camp, V.E., Tolan, T.L., Martin, B.S., 2013. The Columbia River flood basalt province: stratigraphy, areal extent, volume, and physical volcanology. In: The Columbia River Flood Basalt Province. Geological Society of America.

Reidel, S.P., Hooper, P.R., Webster, G.D., Camp, V.E., 1992. Geologic Map of Southeastern Asotin County, Washington. Washington Division of Geology and Earth Resources, Olympia. Washington Geologic Map 6M-40.

Reidel, S.P., Tolan, T.L., 2013. The Grande Ronde Basalt, Columbia River Basalt Group. In: Geological Society of America Special Paper, vol. 497, pp. 117–153.

Rivalta, E., Taisne, B., Bunger, A., Katz, R., 2015. A review of mechanical models of dike propagation: schools of thought, results and future directions. Tectonophysics 638, 1–42. https://doi.org/10.1016/j.tecto.2014.10.003.

Ross, M.E., 1983. Chemical and mineralogic variations within four dikes of the Columbia River Basalt Group, southeastern Columbia Plateau. GSA Bull. 94, 1117–1126. https://doi.org/10.1130/0016-7606(1983)94<1117:CAMVWF>2.0.CO;2.

Sawlan, M.G., 2017. Alteration, mass analysis, and magmatic compositions of the Sentinel Bluffs Member, Columbia River flood basalt province. Geosphere 14, 286–303. https://doi.org/10.1130/GES01188.1.

Schmidt, A., Skeffington, R.A., Thordarson, T., Self, S., Forster, P.M., Rap, A., Ridgwell, A., Fowler, D., Wilson, M., Mann, G.W., 2016. Selective environmental stress from sulphur emitted by continental flood basalt eruptions. Nat. Geosci. 9, 77–82. https://doi.org/10.1038/ngeo2588.

Schoene, B., Eddy, M.P., Samperton, K.M., Keller, C.B., Keller, G., Adatte, T., Khadri, S.F., 2019. U-Pb constraints on pulsed eruption of the Deccan Traps across the end-Cretaceous mass extinction. Science 363, 862–866.

Self, S., Jay, A.E., Widdowson, M., Keszthelyi, L.P., 2008. Correlation of the Deccan and Rajahmundry Trap lavas: are these the longest and largest lava flows on Earth? J. Volcanol. Geotherm. Res. 172, 3–19. https://doi.org/10.1016/j.jvolgeores.2006.11.012.

Sprain, C.J., Renne, P.R., Vanderkluysen, L., Pande, K., Self, S., Mittal, T., 2019. The eruptive tempo of Deccan volcanism in relation to the Cretaceous-Paleogene boundary. Science 363, 866. https://doi.org/10.1126/science.aav1446.

Taubeneck, W.H., 1970. Dikes of Columbia River basalt in northeastern Oregon, western Idaho, and southeastern Washington. In: Proc. 2nd Columbia River Basalt Symposium. Eastern Washington State College Press, Cheney, WA, pp. 73–96.

Tauxe, L., Shaar, R., Jonestrask, L., Swanson-Hysell, N., Minnett, R., Koppers, A., Constable, C., Jarboe, N., Gaastra, K., Fairchild, L., 2016. PmagPy: software package for paleomagnetic data analysis and a bridge to the Magnetics Information Consortium (MagIC) Database. Geochem. Geophys. Geosyst. 17, 2450–2463. https://doi.org/10.1002/2016GC006307.

Thiele, S.T., Cruden, A.R., Zhang, X., Micklethwaite, S., Matchan, E.L., 2021. Reactivation of magma pathways: insights from field observations, geochronology, geomechanical tests, and numerical models. J. Geophys. Res., Solid Earth 126, e2020JB021477. https://doi.org/10.1029/2020JB021477.

Thordarson, T., Self, S., 1996. Sulfur, chlorine and fluorine degassing and atmospheric loading by the Roza eruption, Columbia River Basalt Group, Washington, USA. J. Volcanol. Geotherm. Res. 74, 49–73. https://doi.org/10.1016/S0377-0273(96)00054-6.

Thordarson, T., Self, S., 1993. The Laki (Skaftár Fires) and Grímsvötn eruptions in 1783–1785. Bull. Volcanol. 55, 233–263. https://doi.org/10.1007/BF00624353.

Thordarson, T., Self, S., 1998. The Roza Member, Columbia River Basalt Group: a gigantic pahoehoe lava flow field formed by endogenous processes? J. Geophys. Res., Solid Earth 103, 27411–27445. https://doi.org/10.1029/98JB01355.

Wylie, J.J., Helfrich, K.R., Dade, B., Lister, J.R., Salzig, J.F., 1999. Flow localization in fissure eruptions. Bull. Volcanol. 60, 432–440. https://doi.org/10.1007/s004450050243.

Yu, Y., Tauxe, L., 2006. Acquisition of viscous remanent magnetization. Phys. Earth Planet. Inter. 159, 32–42. https://doi.org/10.1016/j.pepi.2006.05.002.